AD-A036 960 ROME AIR DEVELOPMENT CENTER GRIFFISS AFB N Y F/G 17/9
EFFECT OF CW-396A RADOME ON THE RADIATION PATTERN OF RECTANGULA--ETC(U)
DEC 76 R L FANTE, P R FRANCHI, R L TAYLOR

UNCLASSIFIED RADC-TR-76-397 NL

1 OF 1
AD A036960

END

DATE
FILMED
4-77

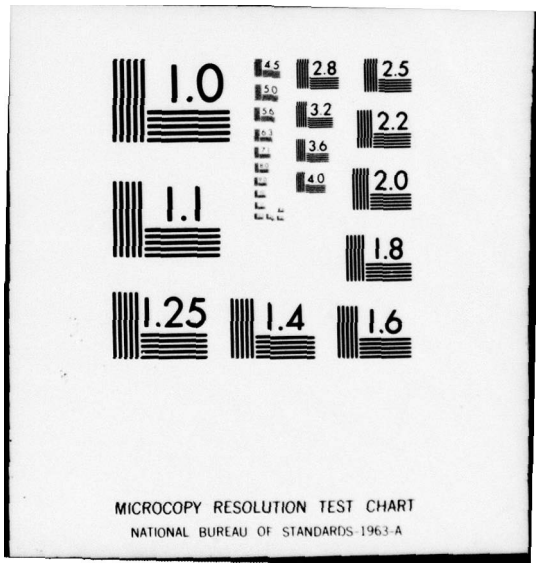
1.0
1.1
1.25
1.4
1.6
1.8
2.0
2.2
2.5
2.8
3.2
3.6
4.0
4.5
5.0
5.6
MICROCOPY RESOLUTION TEST CHART
NATIONAL BUREAU OF STANDARDS-1963-A

RADC-TR-76-397
IN-HOUSE REPORT
DECEMBER 1976

Effect of CW-396A Radome on the Radiation Pattern of Rectangular Antennas

RONALD L FANTE
PETER R. FRANCHI
RICHARD L. TAYLOR

ROME AIR DEVELOPMENT CENTER
AIR FORCE SYSTEMS COMMAND
GRIFFISS AIR FORCE BASE, NEW YORK 13441

This report has been reviewed by the RADC Information Office (OI) and is releasable to the National Technical Information Service (NTIS). At NTIS it will be releasable to the general public, including foreign nations.

This technical report has been reviewed and approved for publication.

APPROVED: Walter Rotman

WALTER ROTMAN
Chief, Microwave Detection Techniques Br.
Electromagnetic Sciences Division

APPROVED: Allan C. Schell

ALLAN C. SCHELL
Acting Chief
Electromagnetic Sciences Division

FOR THE COMMANDER: John P. Huss

Plans Office

Unclassified

SECURITY CLASSIFICATION OF THIS PAGE (When Data Entered)

REPORT DOCUMENTATION PAGE

READ INSTRUCTIONS BEFORE COMPLETING FORM

1. REPORT NUMBER: RADC-TR-76-397	2. GOVT ACCESSION NO.
3. RECIPIENT'S CATALOG NUMBER	
4. TITLE (and Subtitle): EFFECT OF CW-396A RADOME ON THE RADIATION PATTERN OF RECTANGULAR ANTENNAS	5. TYPE OF REPORT & PERIOD COVERED: ~~In-House~~. Technical report
	6. PERFORMING ORG. REPORT NUMBER
7. AUTHOR(s): Ronald L. Fante, Peter R. Franchi, and Richard L. Taylor	8. CONTRACT OR GRANT NUMBER(s)
9. PERFORMING ORGANIZATION NAME AND ADDRESS: Deputy for Electronic Technology (RADC/ETEP) Hanscom AFB Massachusetts 01731	10. PROGRAM ELEMENT, PROJECT, TASK AREA & WORK UNIT NUMBERS: 61102F, 23051401, J4
11. CONTROLLING OFFICE NAME AND ADDRESS: Deputy for Electronic Technology (RADC/ETEP) Hanscom AFB Massachusetts 01731	12. REPORT DATE: December 1976
	13. NUMBER OF PAGES: 32
14. MONITORING AGENCY NAME & ADDRESS(if different from Controlling Office)	15. SECURITY CLASS. (of this report): Unclassified
	15a. DECLASSIFICATION/DOWNGRADING SCHEDULE

16. DISTRIBUTION STATEMENT (of this Report)

Approved for public release; distribution unlimited.

17. DISTRIBUTION STATEMENT (of the abstract entered in Block 20, if different from Report)

18. SUPPLEMENTARY NOTES

19. KEY WORDS (Continue on reverse side if necessary and identify by block number)

Antennas
Radomes
Radiation

20. ABSTRACT (Continue on reverse side if necessary and identify by block number)

We have studied the effect of the CW-396A radome on the radiation pattern of a number of different rectangular antennas. We have found that this radome produces grating lobes, which are approximately 30 dB below the main beam level at L-band and approximately 23 dB lower at S-band. A Fortran listing of the computer program used is included in this report.

309 050

DD FORM 1 JAN 73 1473 EDITION OF 1 NOV 65 IS OBSOLETE

Unclassified

SECURITY CLASSIFICATION OF THIS PAGE (When Data Entered)

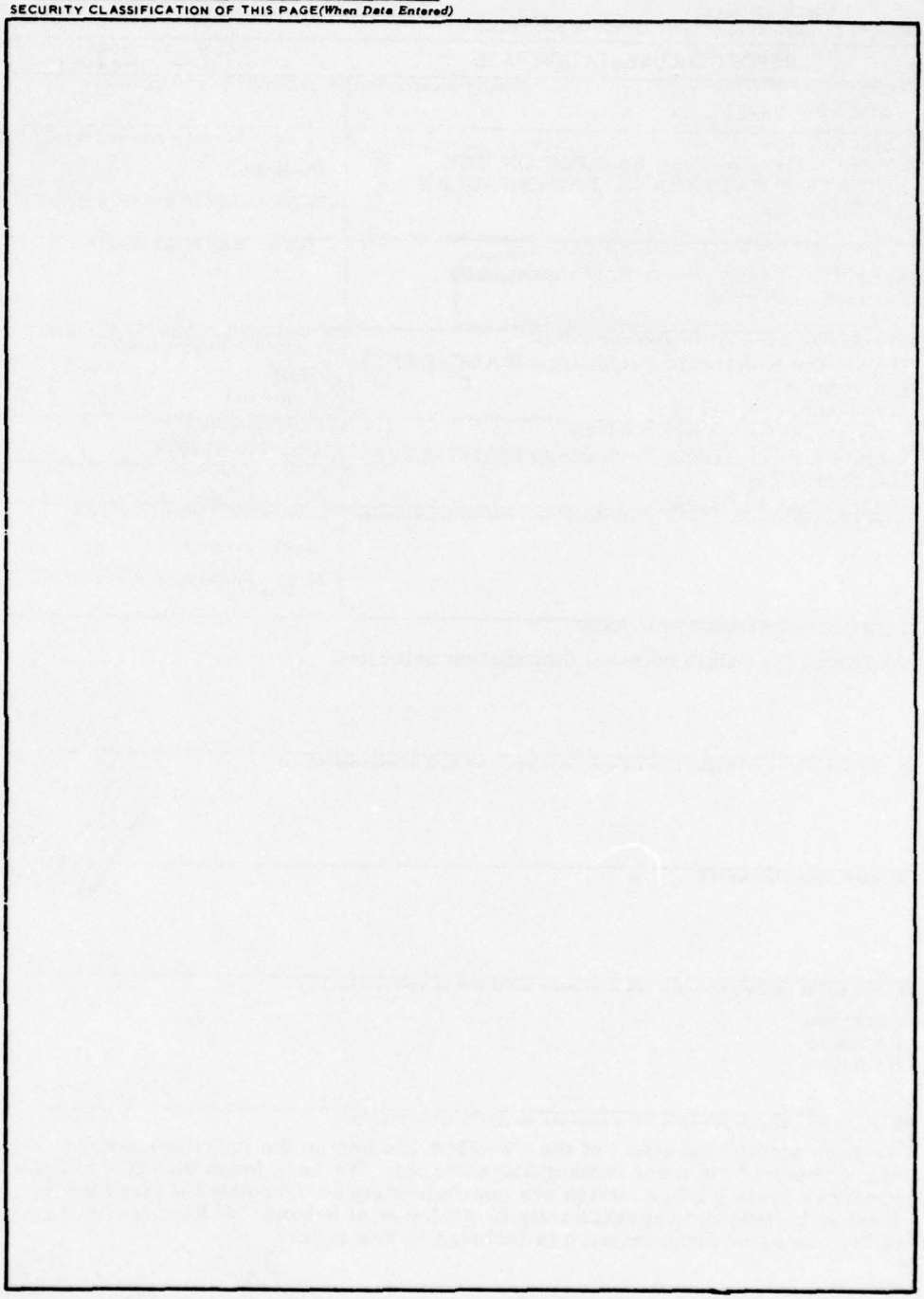

6/2012

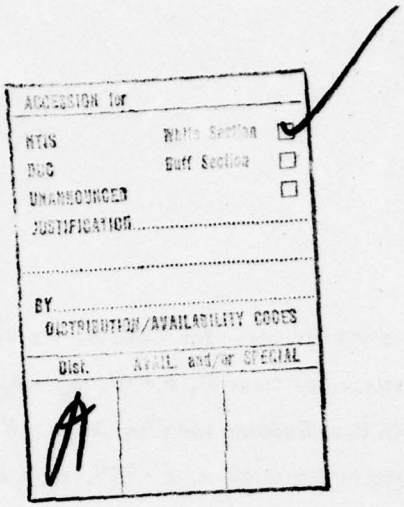

Contents

Illustrations

Illustrations

Effect of CW-396A Radome on the Radiation Pattern of Rectangular Antennas

1. ANALYSIS

In this report we will present some results showing the effect of a CW-396A radome on the radiation pattern of a rectangular aperture. It is well known that in the absence of the radome the radiated power can be written as

$$P_v = A\,(1 - \sin^2\theta \sin^2\phi)\left|\iint_S \underline{K}_s\, e^{ik(x \sin\theta\cos\phi + y \sin\theta \sin\phi)}\, dx\, dy\right|^2, \quad (1)$$

where A is a constant, $\underline{K}_s$ is the electric or magnetic surface current on the radiator, S is the radiator surface area, and θ and ϕ are defined in Figure 1.

Now suppose this antenna is placed inside a CW-396A radome. It has been demonstrated elsewhere that for this type of radome only the radome ribs significantly influence the radiation pattern, and the effect of the radome panels and bolts can be neglected (at least, for frequencies up to and including S-band). For purposes of calculation we have found it convenient to assume that the near fields of the antenna are still collimated as they pass through the radome. Furthermore, we assume that over the intersection of this collimated beam and the radome, the

(Received for publication 29 December 1976)

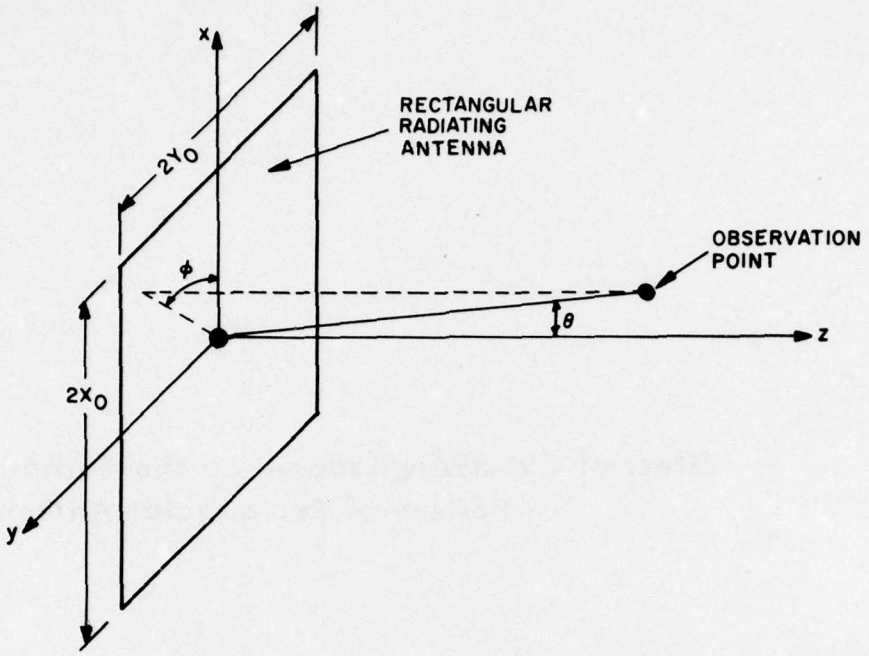

Figure 1. Antenna Geometry

radome surface is nearly flat so that it can be approximated by a rib structure which is periodic in x and y, as shown in Figure 2.

In order to calculate the effect of this approximate radome structure on the radiation field we employ the equivalent current method. Using this method we calculate the field which is scattered by each radome rib and then approximate that rib by a current sheet which produces the same radiation field. This current sheet is then projected back onto the antenna so that the net antenna current is the original surface current K_s plus the surface currents K_R due to all the radome ribs that are projected back onto the antenna. Therefore, in place of Eq. (1) we get

$$P_R = A'(1-\sin^2\theta\sin^2\phi)\left|\iint_S K_s\, e^{ik(x\sin\theta\cos\phi + y\sin\theta\sin\phi)}\,dx\,dy\right. \tag{2}$$

$$\left. + \iint_S K_R\, e^{ik(x\sin\theta\cos\phi + y\sin\theta\sin\phi + h\cos\theta)}\,dx\,dy\right|,$$

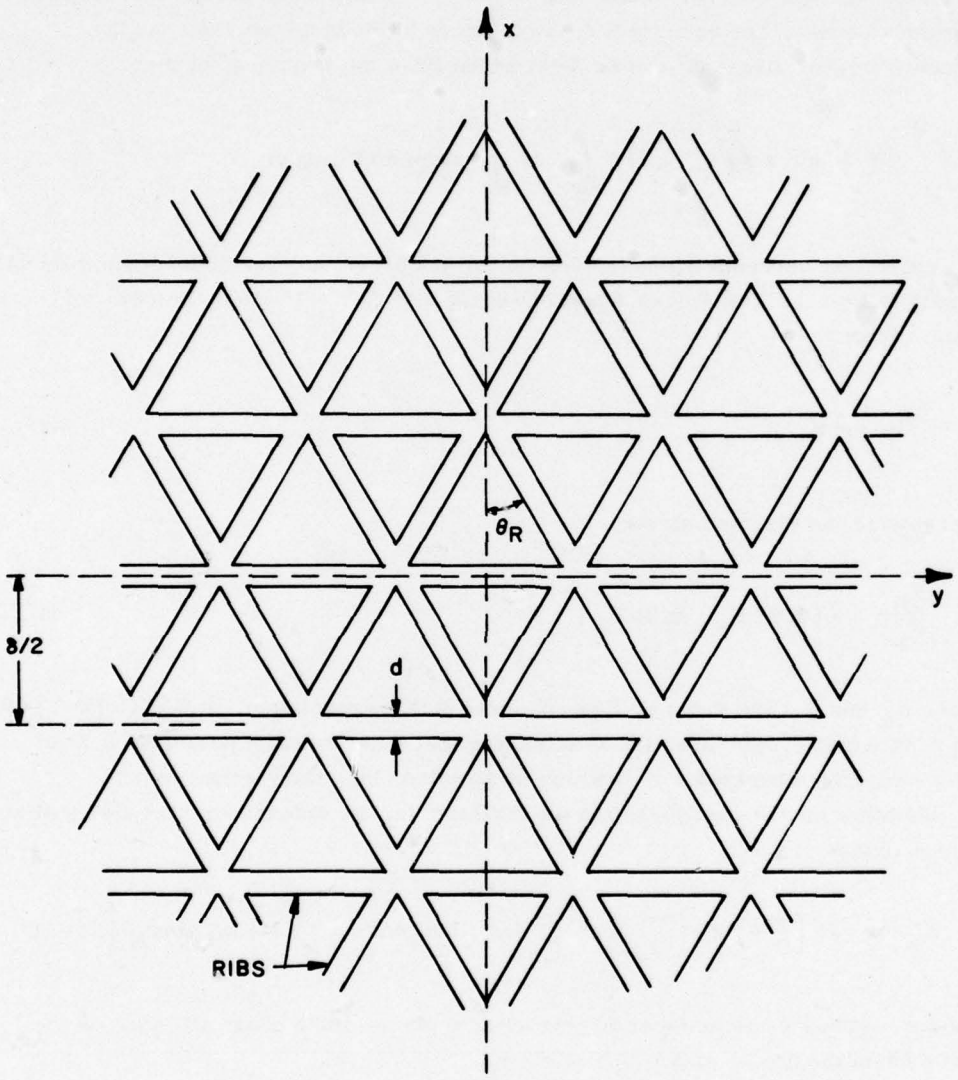

Figure 2. Approximate Planar Radome Geometry: for CW-396A we have $\delta = 117.88''$ and $\theta_R = 32^o$

where the equivalent current K_R is nonzero only over those portions of the surface S upon which a radome rib is projected and the factor exp (ikh cos θ) accounts for the phase shift between the actual location of the radome ribs and their projection onto the antenna. The quantity h is the distance between the antenna and the radome surface. Also, A' can be determined from the requirement that

$$\int_0^{2\pi} d\phi \int_0^{\pi} \sin\theta \, d\theta \, P_v(\theta,\phi) = \int_0^{2\pi} d\phi \int_0^{\pi} \sin\theta \, d\theta \, P_R(\theta,\phi) \ .$$

The equivalent currents K_R have been calculated previously for both L- and S-band signals in Eq. (18) and Tables 1 to 4 of report RADC-TR-76-379. For the horizontal struts

$$\frac{\underline{K}_R}{|\underline{K}_s|} = \hat{x} \, K_{\parallel} \ , \tag{3}$$

whereas for the diagonal struts

$$\frac{\underline{K}_R}{|\underline{K}_s|} = \hat{x} \, [\, 0.53 \, K_{\parallel} + 0.85 \, K_{\perp} \,] \ , \tag{4}$$

where $K_{\parallel}$ and $K_{\perp}$ are given by Eqs. (2) and (22), respectively, in RADC-TR-76-379, and $\hat{x}$ is a unit vector along the x-axis (note that a horizontally polarized E field gives a magnetic current $\hat{z} \times \underline{E}$ which is directed along the vertical axis).

We have not yet specified what we shall use for the antenna current distribution $\underline{K}_s$; we choose

$$K_s = \hat{x} \cos\left(\frac{\pi x}{2x_o}\right) \cos\left(\frac{\pi y}{2y_o}\right) \exp\left\{ -ik(x \sin\theta_B \cos\phi_B + y \sin\theta_B \sin\phi_B) \right\} \ . \tag{5}$$

The current has a cosine taper in both x and y planes and a phase tilt such as to give a beam maximum at $\theta = \theta_B$ and $\phi = \phi_B$.

2. RESULTS

If we assume that the antenna lies at the center of the CW-396A radome it is appropriate to choose h = 324 in. Also, the separation $\delta/2$ between horizontal ribs is 58.94 in. and the angle θ_R defined in Figure 2 is 32°. For the case when

there is no beam displacement (that is, $\theta_B = \phi_B = 0$) we have calculated the effect of the radome on the antenna pattern for the cases listed in Table 1.

Table 1. Effect of Radome on Antenna Pattern

Case	Frequency (GHz)	$2x_o$ (Inches)	$2y_o$ (Inches)	ϕ (Degrees)	See Figure
A	1.35	360	180	0	3
	1.35	360	180	32	4
	1.35	360	180	58	5
	1.35	360	180	90	6
B	3.15	240	144	0	7
	3.15	240	144	32	8
	3.15	240	144	58	9
	3.15	240	144	90	10
C	3.30	312	168	0	11
	3.30	312	168	58	12
	3.30	312	168	90	13

In plotting P_R in Figures 3 to 13 we have normalized P_R so that $P_R(\theta = 0) = P_V(\theta = 0)$. This of course ignores the power loss in the main beam caused by power being scattered by the radome into the sidelobes. By using the conservation equation

$$\int_0^{2\pi} d\phi \int_0^{2\pi} \sin\theta \, d\theta \, [\, P_R(\theta,\phi) - P_v(\theta,\phi) \,] = 0 \quad ,$$

it is possible to estimate the loss in gain caused by the radome, as shown in Table 2.

Table 2. Estimated Loss in Gain

Case	Approximate Gain Loss (dB)
A	0.1
B	1.0
C	1.3

It is interesting to note from Figures 3, 7, and 11 that the grating lobes caused by the horizontal radome ribs are about 30 dB below the main beam level at L-band and about 23 to 24 dB below at S-band. The diagonal radome ribs produce grating lobes at $\phi = 58^{\circ}$, as is clear from Figures 5, 9, and 12. These are about 35 dB below the main beam level at L-band and about 26 to 30 dB below at S-band. There are no appreciable grating lobes for any other values of ϕ in the range $0 \leq \phi \leq 90^{\circ}$ (of course there are grating lobes in the $\phi = 122^{\circ}$, 180°, 238°, and 302° planes), as is clear from Figures 4, 6, 8, 10, and 13.

We have also studied the radiation pattern in the $\phi = 0^{\circ}$ plane for the case when there is a 5° main beam tilt in the vertical plane (that is, $\theta_B = 5^{\circ}$, $\phi_B = 0$). These results are shown in Figures 14 to 16.

3. CONCLUSIONS AND DISCUSSION

The CW-396A radome can produce grating lobes in the vertical plane which are about 30 dB below the main beam at L-band and about 23 to 24 dB below the main beam at S-band. The radome produces about a 0.1 dB loss in gain at L-band and about a 1 dB loss in gain at S-band.

Finally, we should note that all the panel sizes on the CW-396A radome are not exactly the same, as we have assumed in our approximate model. These slight size differences would tend to broaden and lower the grating lobes by a small amount (about a dB). We have also considered the effect of radome curvature. This effect is shown in Figures 17 to 19. Upon comparing Figures 17 to 19 with Figures 3, 7, and 11 we see that the effect of the radome curvature is small.

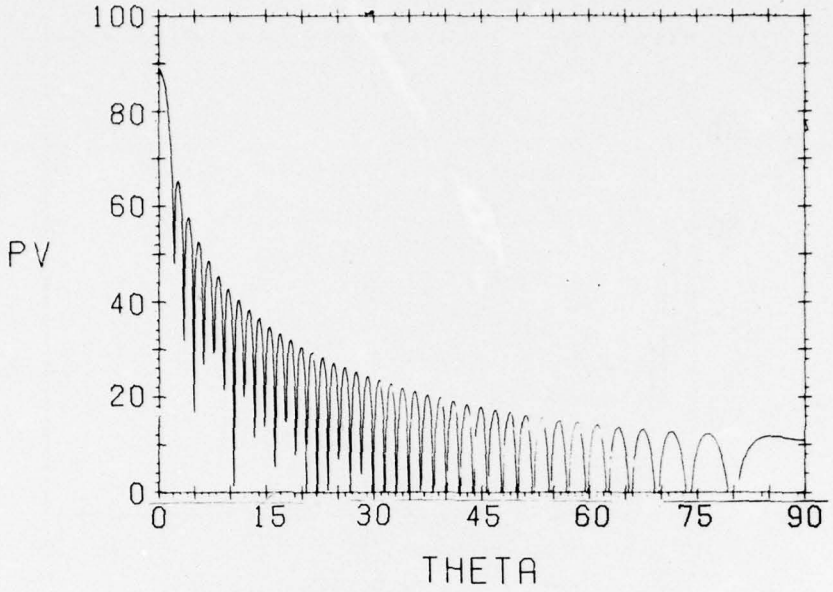

Figure 3a. Vacuum Radiation Pattern for Case A, $\phi = 0^o$, $\theta_B = \phi_B = 0^o$

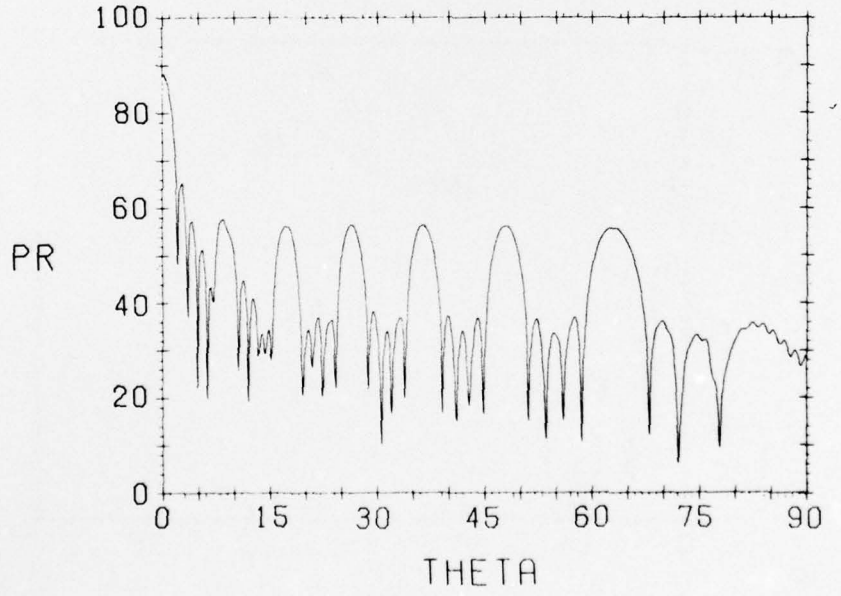

Figure 3b. Radiation Pattern with Flat Radome for Case A, $\phi = 0^o$, $\theta_B = \phi_B = 0^o$

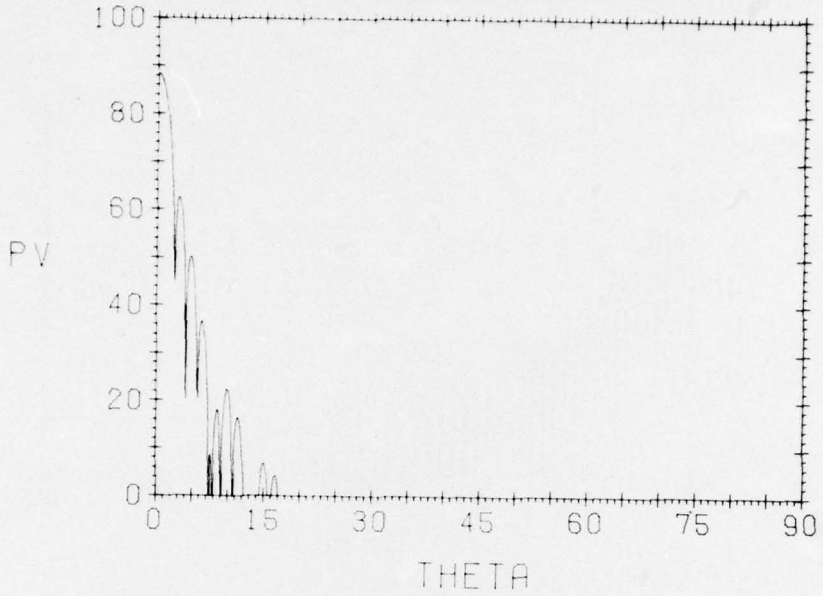

Figure 4a. Vacuum Radiation Pattern for Case A, $\phi = 32^{o}$, $\theta_B = \phi_B = 0^{o}$

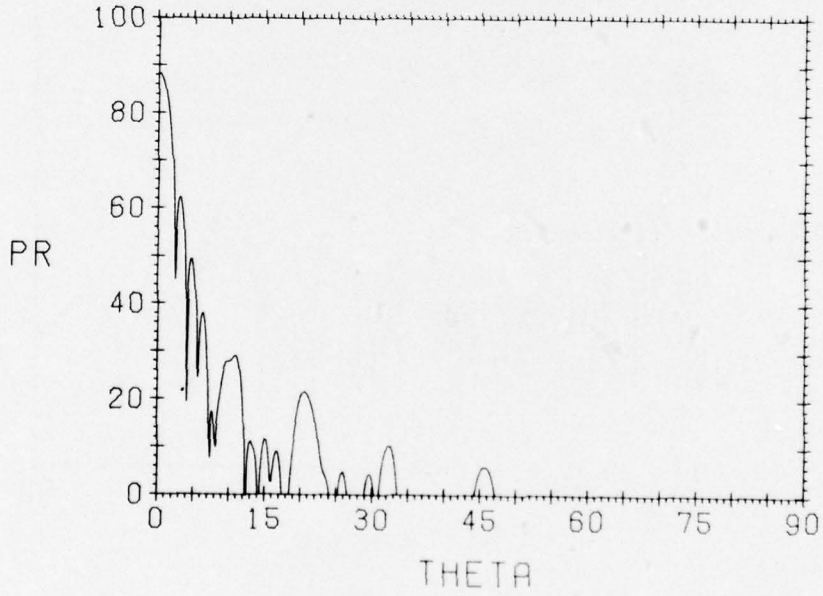

Figure 4b. Radiation Pattern with Flat Radome for Case A, $\phi = 32^{o}$, $\theta_B = \phi_B = 0^{o}$

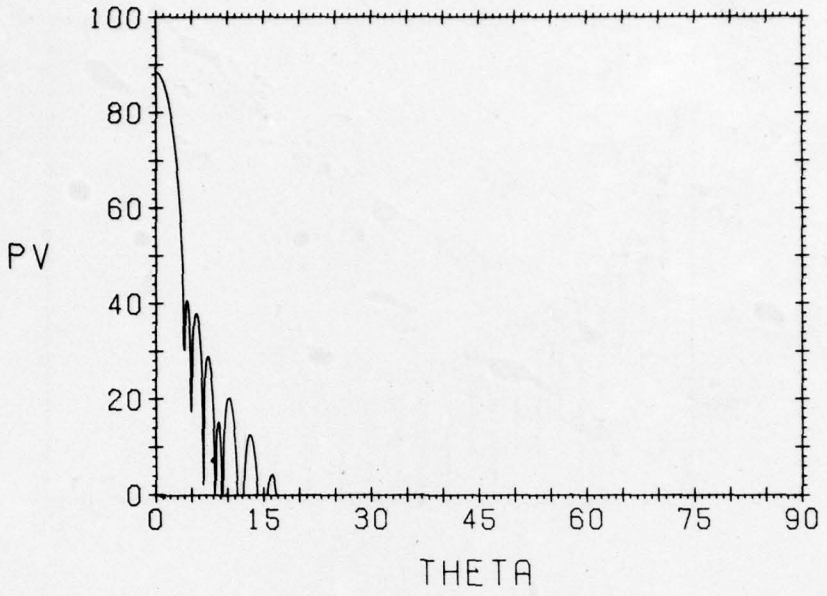

Figure 5a. Vacuum Radiation Pattern for Case A, $\phi = 58^{o}$, $\theta_B = \phi_B = 0^{o}$

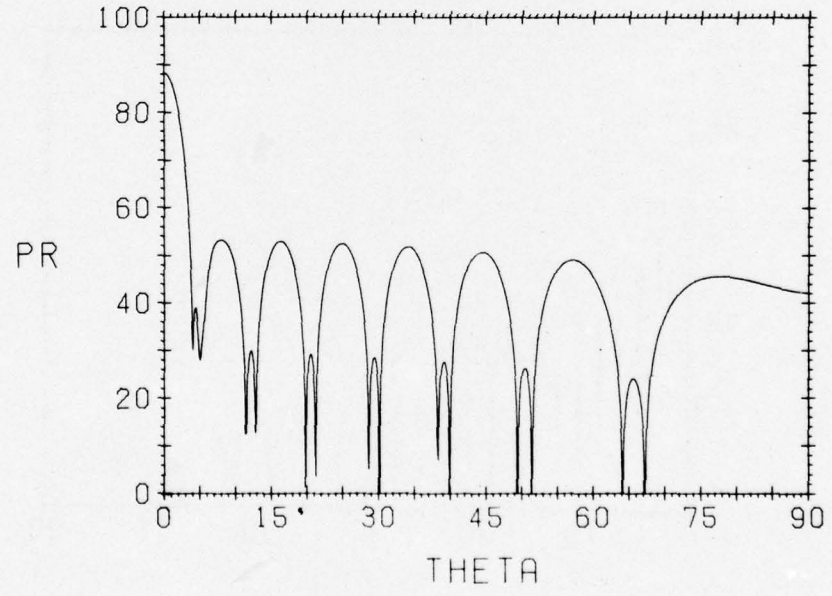

Figure 5b. Radiation Pattern with Flat Radome for Case A, $\phi = 58^{o}$, $\theta_B = \phi_B = 0^{o}$

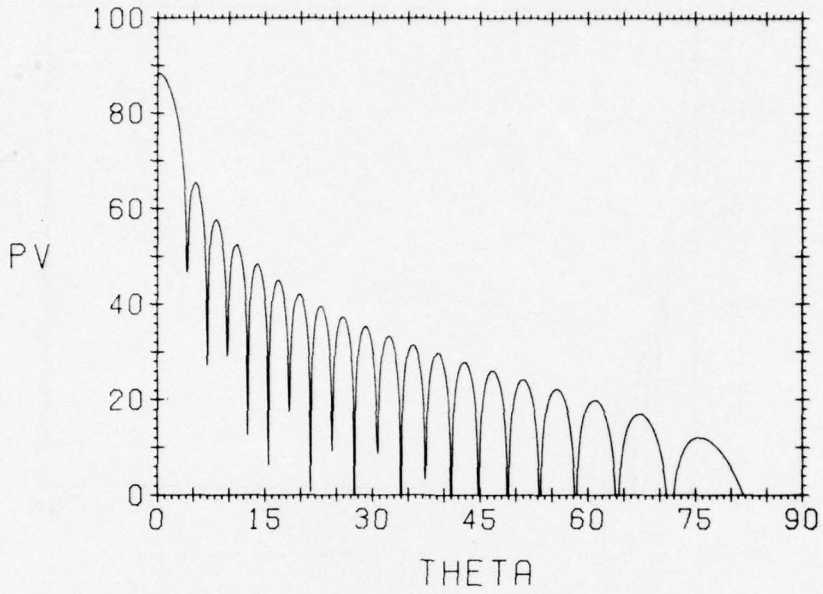

Figure 6a. Vacuum Radiation Pattern for Case A, $\phi = 90^{o}$, $\theta_B = \phi_B = 0^{o}$

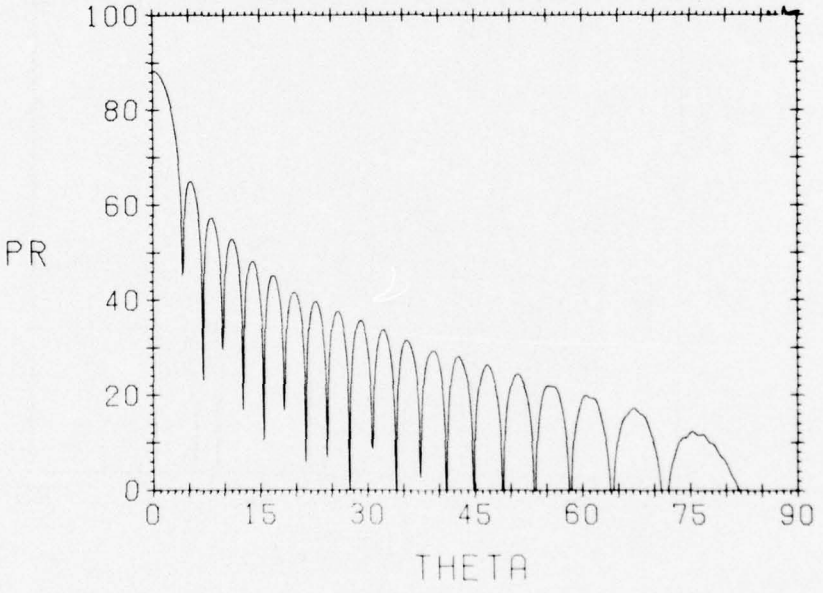

Figure 6b. Radiation Pattern with Flat Radome for Case A, $\phi = 90^{o}$, $\theta_B = \phi_B = 0^{o}$

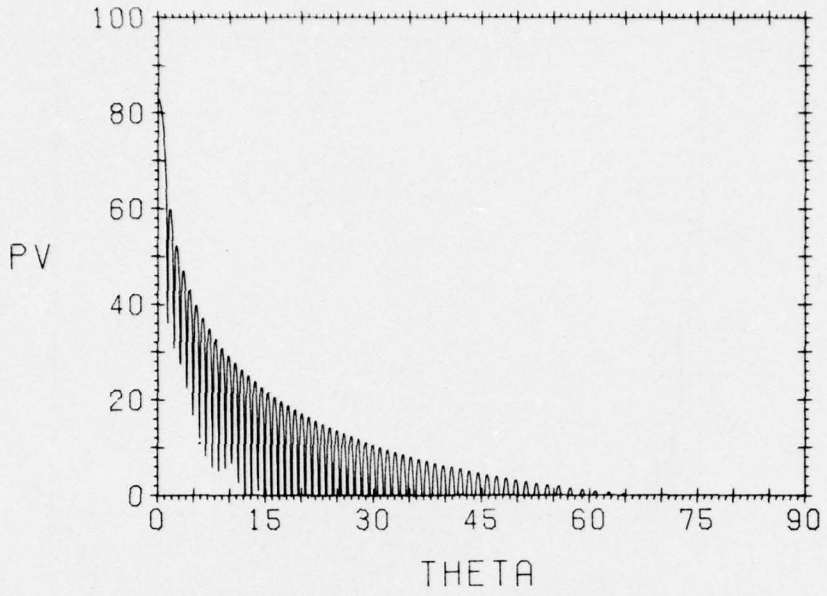

Figure 7a. Vacuum Radiation Pattern for Case B, $\phi = 0^{o}$, $\theta_B = \phi_B = 0^{o}$

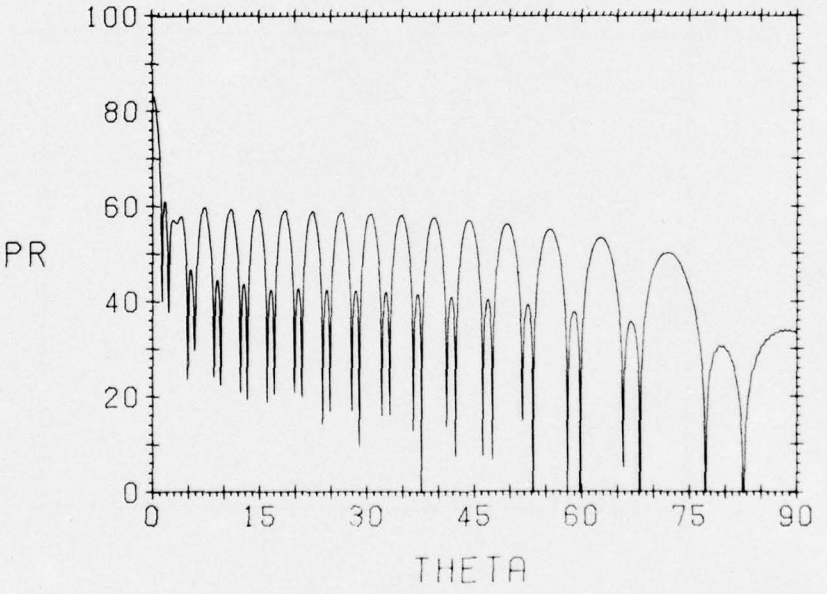

Figure 7b. Radiation Pattern with Flat Radome for Case B, $\phi = 0^{o}$, $\theta_B = \phi_B = 0^{o}$

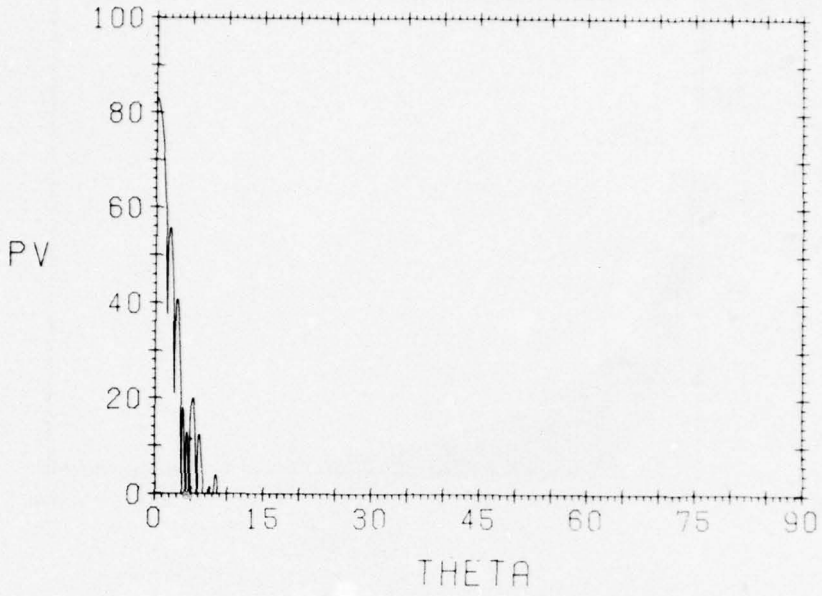

Figure 8a. Vacuum Radiation Pattern for Case B, $\phi = 32^{o}$, $\theta_B = \phi_B = 0^{o}$

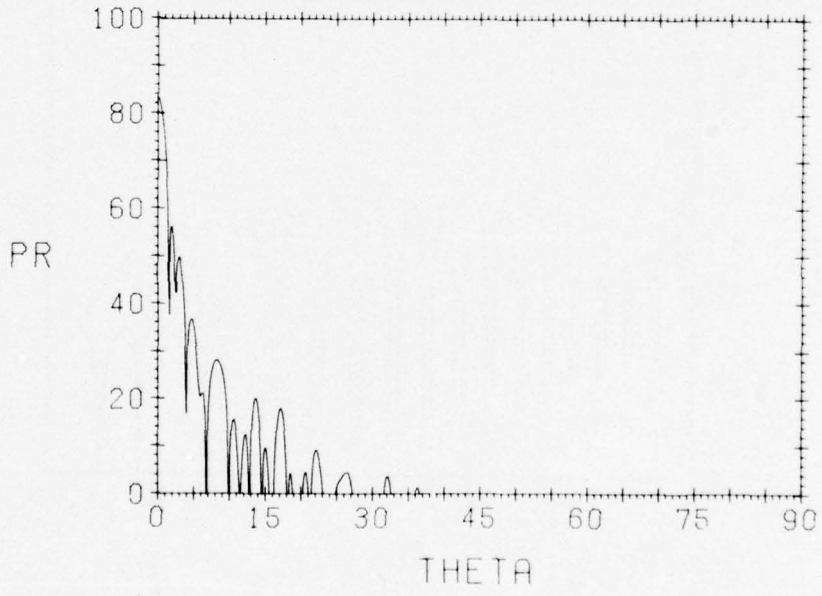

Figure 8b. Radiation Pattern with Flat Radome for Case B, $\phi = 32^{o}$, $\theta_B = \phi_B = 0^{o}$

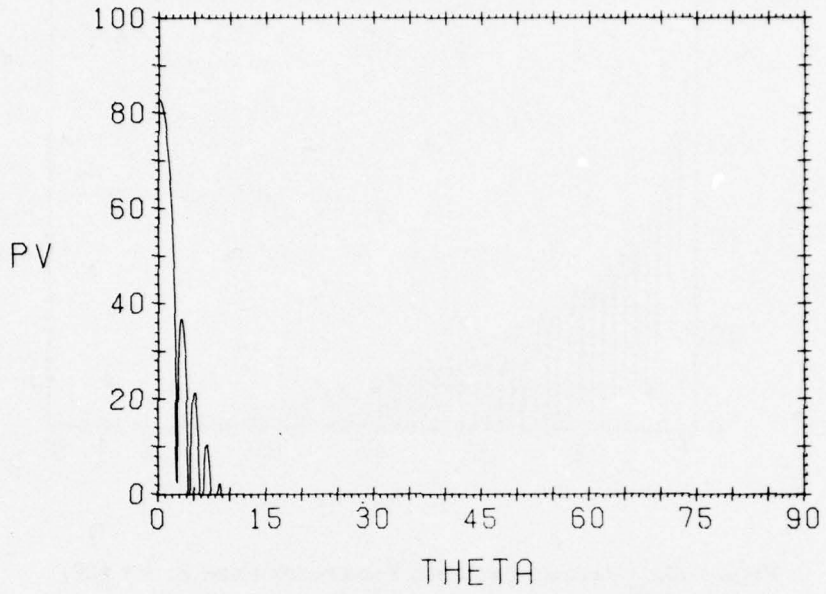

Figure 9a. Vacuum Radiation Pattern for Case B, $\phi = 58^{o}$, $\theta_B = \phi_B = 0^{o}$

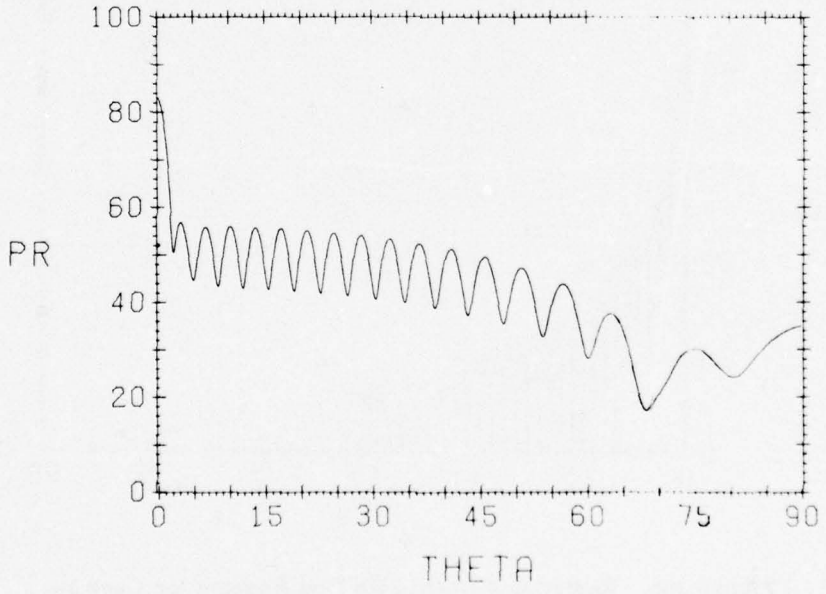

Figure 9b. Radiation Pattern with Flat Radome for Case B, $\phi = 58^{o}$, $\theta_B = \phi_B = 0^{o}$

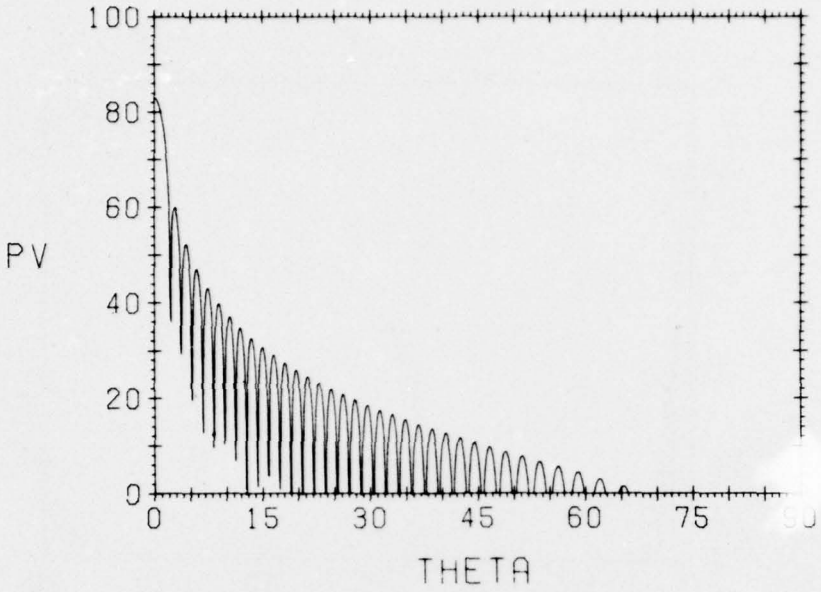

Figure 10a. Vacuum Radiation Pattern for Case B, $\phi = 90^{o}$, $\theta_B = \phi_B = 0^{o}$

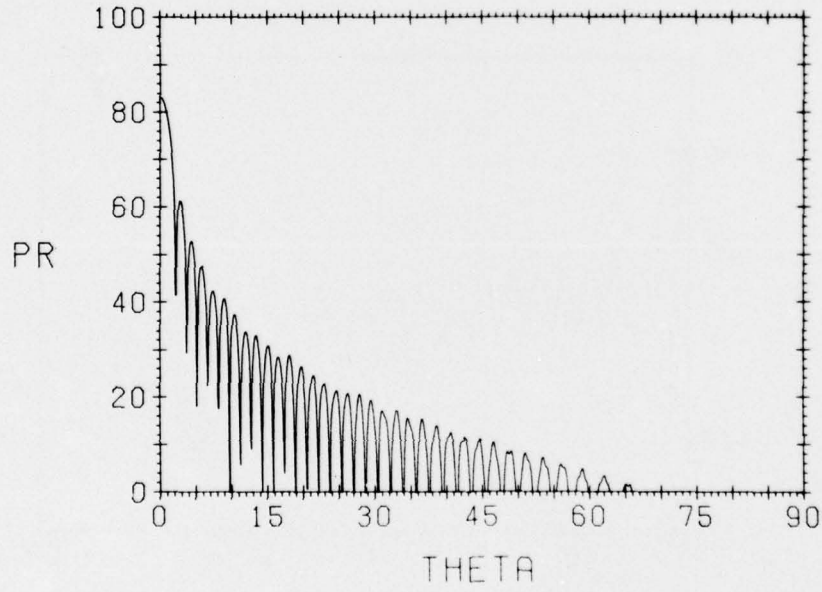

Figure 10b. Radiation Pattern with Flat Radome for Case B, $\phi = 90^{o}$, $\theta_B = \phi_B = 0^{o}$

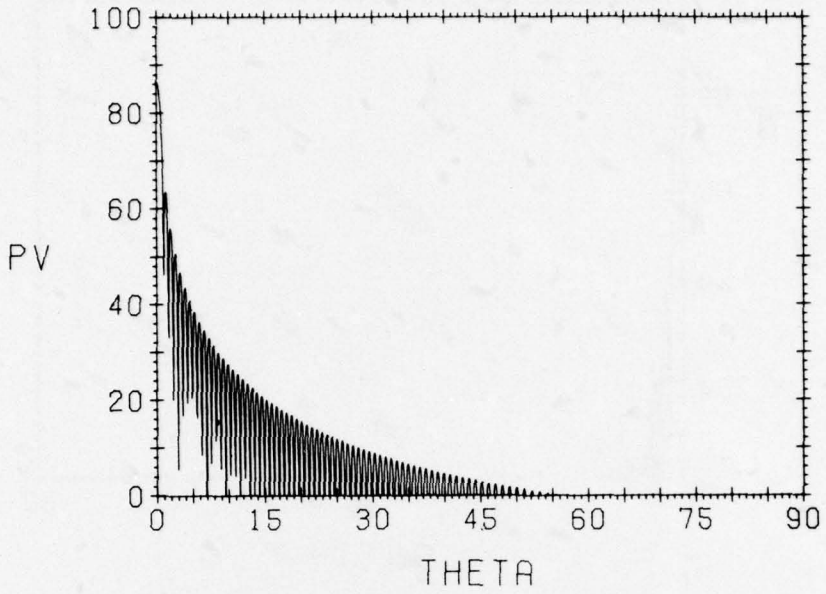

Figure 11a. Vacuum Radiation Pattern for Case C, $\phi = 0^{o}$, $\theta_B = \phi_B = 0^{o}$

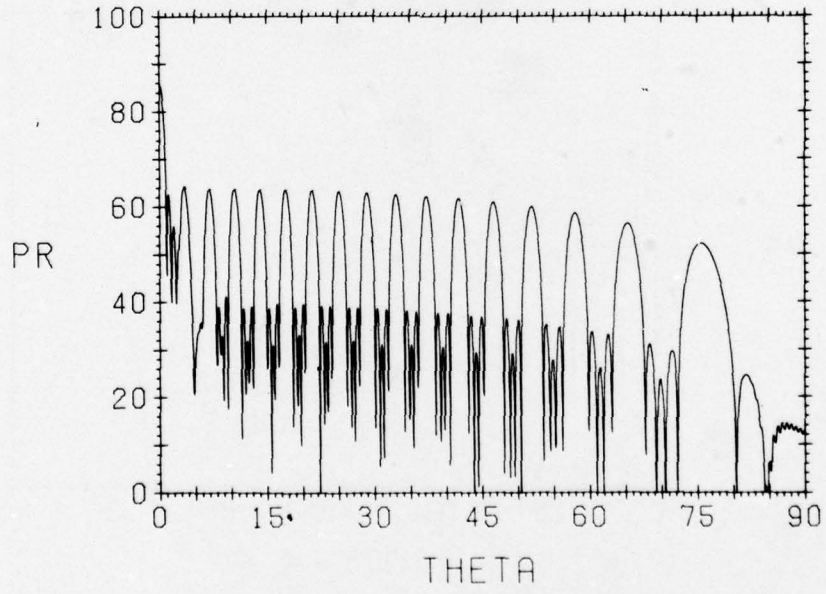

Figure 11b. Radiation Pattern with Flat Radome for Case C, $\phi = 0^{o}$, $\theta_B = \phi_B = 0^{o}$

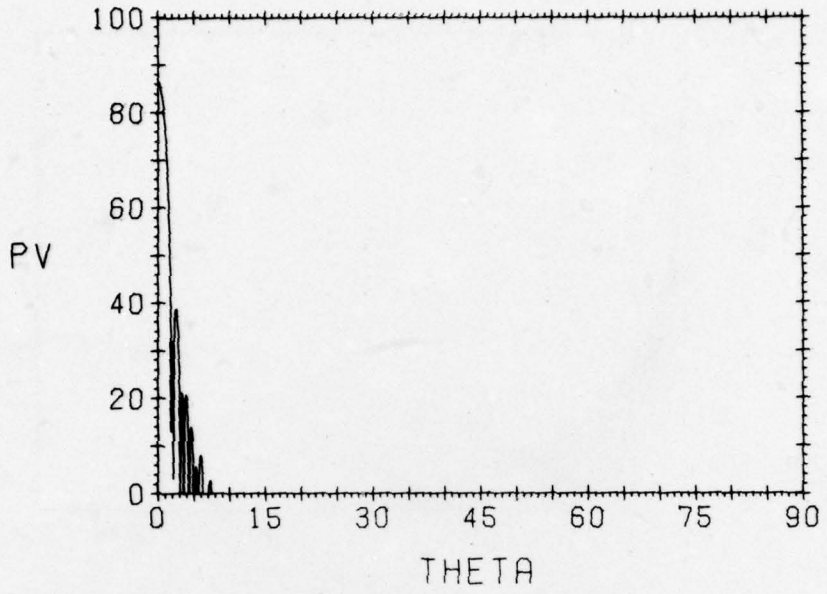

Figure 12a. Vacuum Radiation Pattern for Case C, $\phi = 58^{o}$, $\theta_B = \phi_B = 0^{o}$

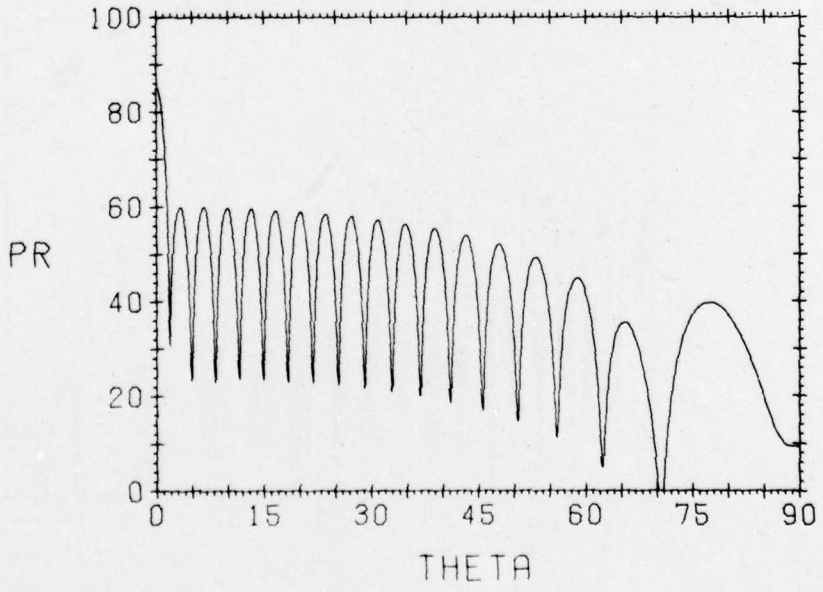

Figure 12b. Radiation Pattern with Flat Radome for Case C, $\phi = 58^{o}$, $\theta_B = \phi_B = 0^{o}$

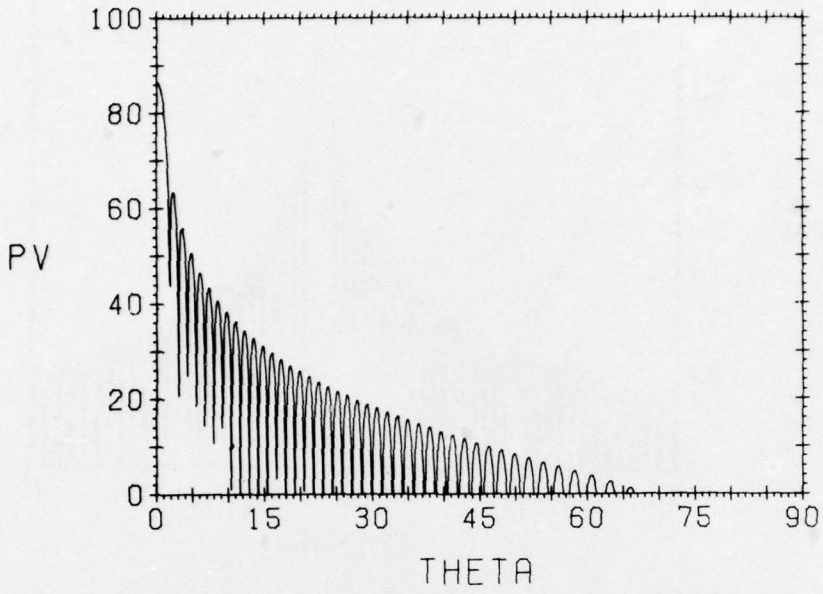

Figure 13a. Vacuum Radiation Pattern for Case C, $\phi = 90^{o}$, $\theta_B = \phi_B = 0^{o}$

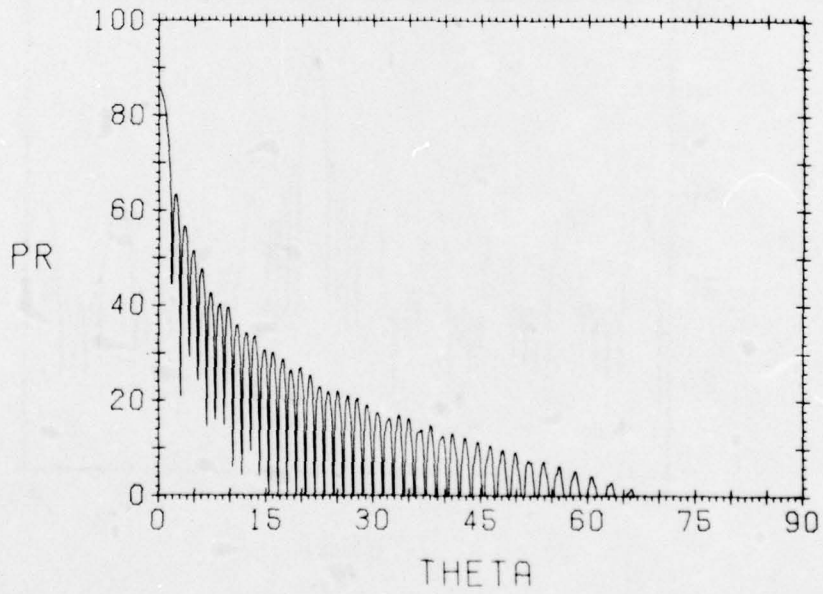

Figure 13b. Radiation Pattern with Flat Radome for Case C, $\phi = 90^{o}$, $\theta_B = \phi_B = 0^{o}$

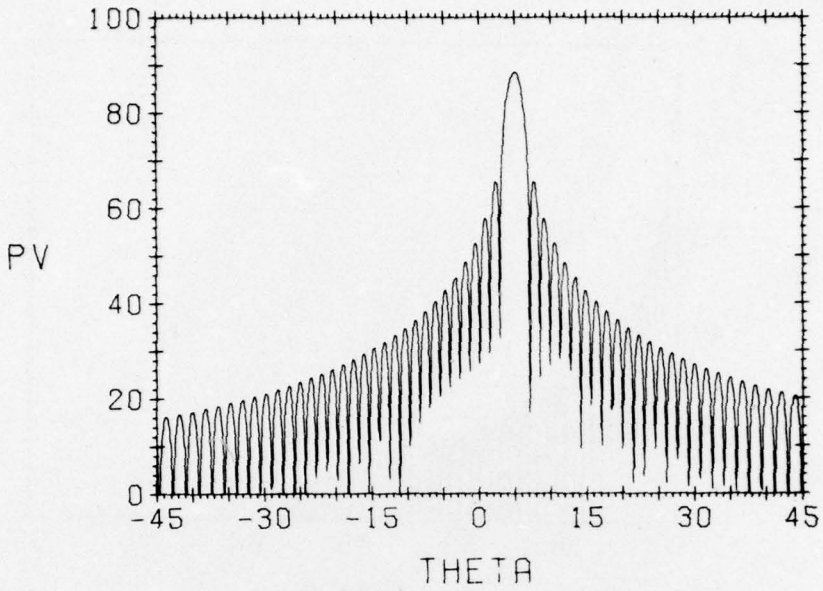

Figure 14a. Vacuum Radiation Pattern for Case A, $\theta_B = 5^o$, $\phi = 0^o$, $\theta_B = 0^o$

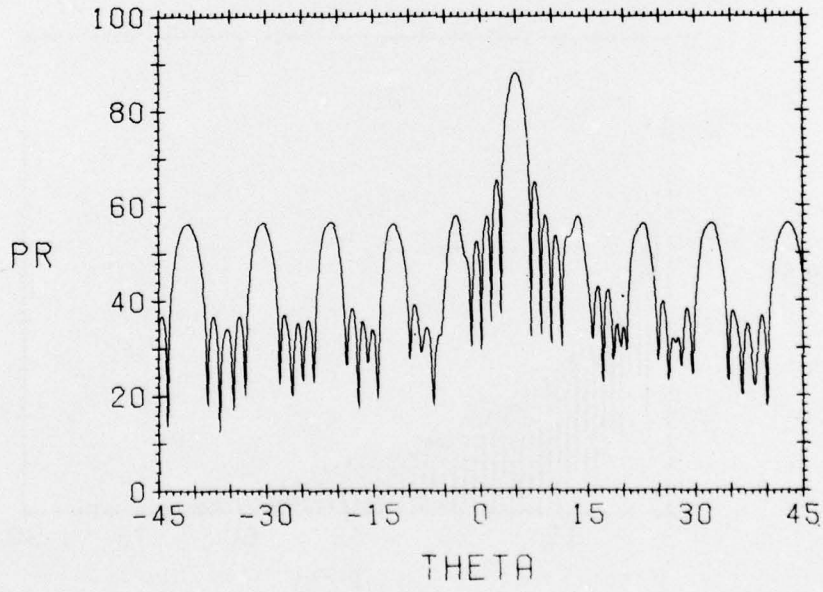

Figure 14b. Radiation Pattern with Flat Radome for Case A, $\theta_B = 5^o$, $\phi = 0^o$, $\phi_B = 0^o$

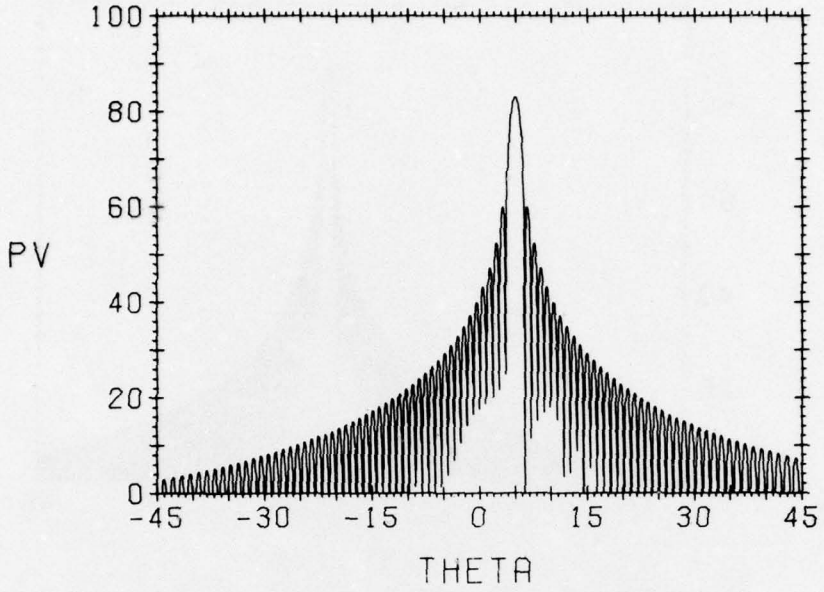

Figure 15a. Vacuum Radiation Pattern for Case B, $\theta_B = 5^o$, $\phi = 0^o$, $\phi_B = 0^o$

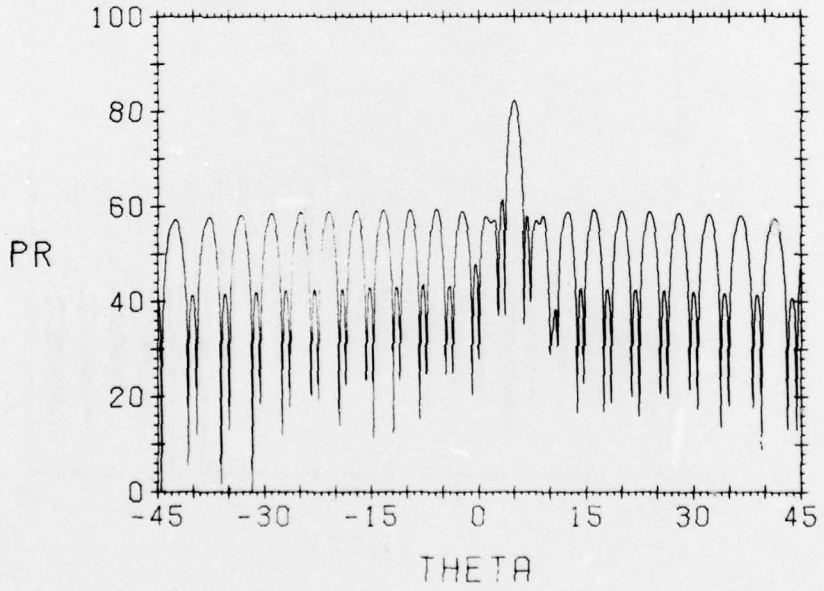

Figure 15b. Radiation Pattern with Flat Radome for Case B, $\theta_B = 5^o$, $\phi = 0^o$, $\phi_B = 0^o$

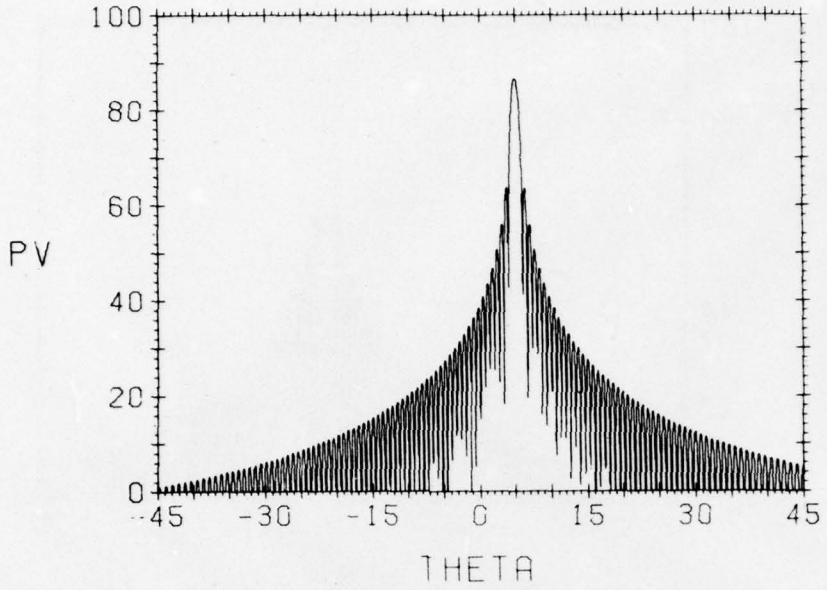

Figure 16a. Vacuum Radiation Pattern for Case C, $\theta_B = 5^o$, $\phi = 0^o$, $\phi_B = 0^o$

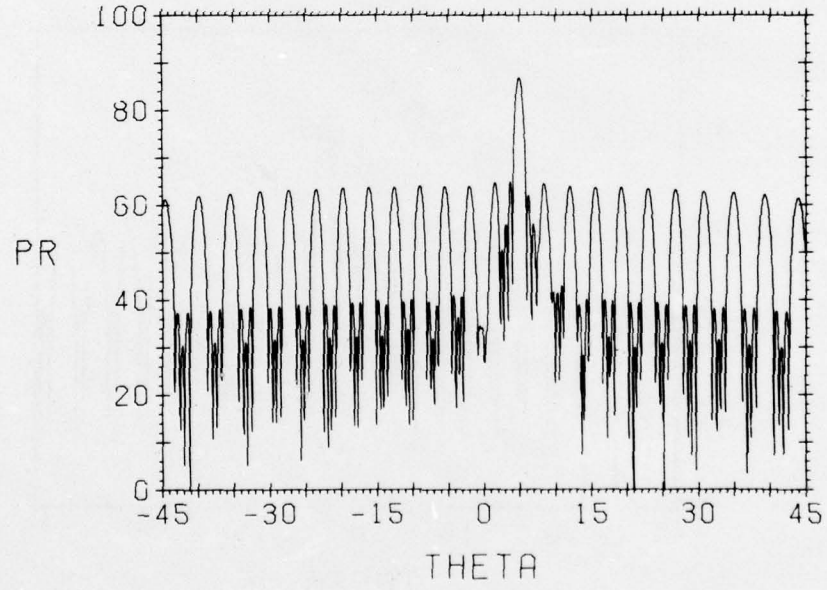

Figure 16b. Radiation Pattern with Flat Radome for Case C, $\theta_B = 5^o$, $\phi = 0^o$, $\phi_B = 0^o$

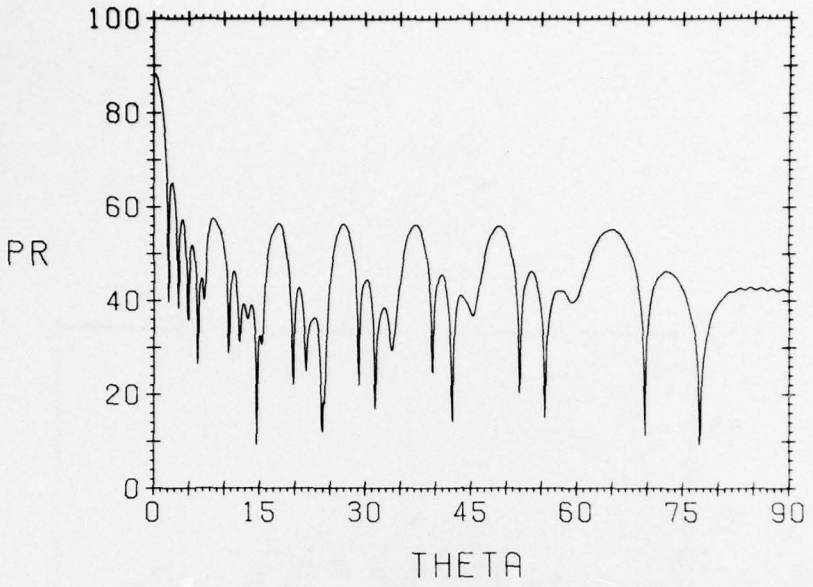

Figure 17. Radiation Pattern with Spherical Radome for Case A, $\phi = \theta_B = \phi_B = 0^o$

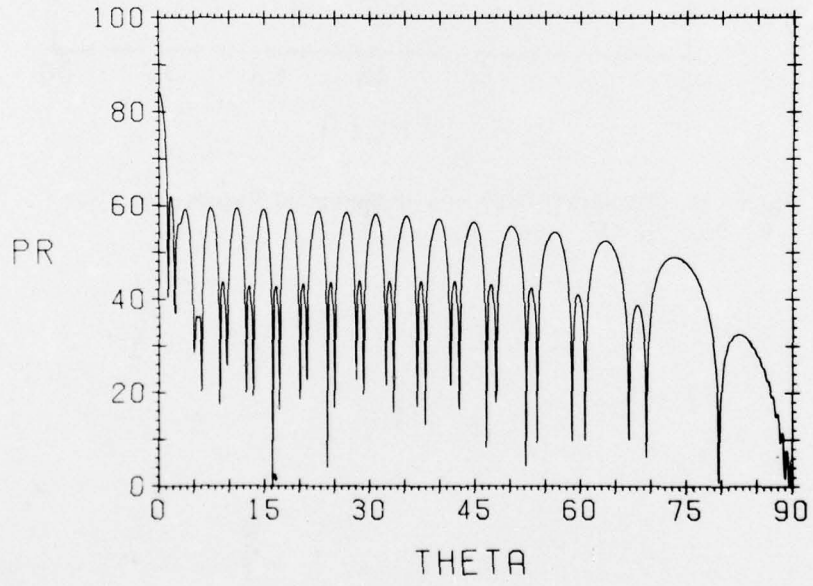

Figure 18. Radiation Pattern with Spherical Radome for Case B, $\phi = \theta_B = \phi_B = 0^o$

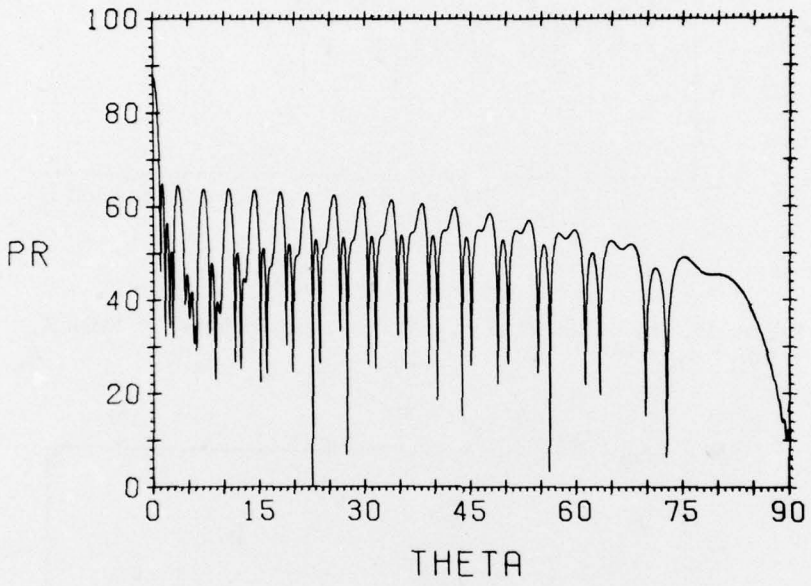

Figure 19. Radiation Pattern with Spherical Radome for Case C, $\phi = \theta_B = \phi_B = 0^o$

Appendix A

Fortran Listing of the Computer Program Used for Calculating Radome Effects

```
      PROGRAM MAIN(INPUT, OUTPUT)
      IMPLICIT COMPLEX(C)
      REAL  K, LAMBDA1, LAMBDA2, LAMBDA3, LAMBDA4
      DIMENSION  NARRAY(6), AMPL(14,2), ANGLE(14,2), CF(7)
      DIMENSION  WW(3), TT(3), LU(3), SS(3)
      DATA  (PI = 3.14159265358979), (KARRAY = 6*(-1) )
      DATA  (AMPL = 0.9199, 0.9578, 1.0398, 1.1651, 1.2929, 1.3873,
     1   1.3949, 1.3334, 0.2782, 0.2755, 0.2765, 0.2805, 0.2857, 0.3492,
     2   1.0364, 0.8293, 1.6219, 1.8056, 1.2738, 1.5761, 2.1850, 0.3625,
     3   0.3302, 0.3469, 0.3409, 0.3279, 0.3336, 0.4166)
      DATA  (ANGLE = -95.0, -102.8, -110.1, -114.1, -114.7, -113.3,
     1   -110.2, -84.5, -89.2, -89.4, -92.9, -94.2, -95.3, -99.0,
     2   -87.1, -132.5, -146.7, -136.3, -145.5, -180.4, -176.5, -84.1,
     3   -95.1, -96.9, -97.5, -101.0, -136.3, -114.6)
      NAMELIST/XINPUT/D, DEL, XO, YO, K, RTHETA, IFE, ITYPE, H, THETAL,
     1   THETAU, DELTH, PHI, PHIB, THETAB
C
C
      CF(CL,A1,A2) = CEXP(CMPLX(0.0,CL*A1) ) - CEXP(CMPLX(0.0,CL*A2) )
C
C
C
C
C     D             RIB THICKNESS (INCHES)
C     DEL           TWICE THE SEPARATION BETWEEN HORIZONTAL RIBS (INCHES)
C     XO            1/2 THE APERTURE VERTICAL DIMENSION (INCHES)
C     YO            1/2 THE APERTURE HORIZONTAL DIMENSION (INCHES)
C     K             WAVENUMBER (RECIPROCAL INCHES)
C     RTHETA        1/2 THE ANGLE BETWEEN DIAGONAL RIBS AT 0 HORIZONTAL
C                         RIB (DEGREES)
C     IFE           FREQUENCY BAND -    1 FOR L-BAND, 2 FOR S-BAND
C     ITYPE         1 FOR PLANAR, 2 FOR SPHERICAL
C     H             DISTANCE FROM ANTENNA TO BACOME (INCHES)
C     THETAL        BEGINNING VALUE OF THETA (DEGREES)
C     THETAU        ENDING VALUE OF THETA (DEGREES)
C     DELTH         THETA INCREMENT (DEGREES)
C     PHI           AZIMUTHAL ANGLE (DEGREES)
C     PHIB          BEAM
C     THETAB             TILT  (DEGREES)
C
C
C
      NARRAY(3) = NARRAY(2) = 0
      CALL SYSTEM(115, NARRAY)
      DEG2RAD = PI / 180.0
      EPS = 4.1
      READ XINPUT
      CALL SSWTCH(3, MSW)
      IF(MSW .EQ. 2)  PRINT XINPUT
      ARCSIN = XO / H
      IF(ITYPE .EQ. 2)  ARCSIN = ASIN(ARCSIN)
      NN = INT(ARCSIN*H/DEL)
      ENN = FLOAT(NN)
      SINPHI = SIN(PHI*DEG2RAD)
      COSPHI = COS(PHI*DEG2RAD)
      COSPHIB = COS(PHIB*DEG2RAD)
      SINPHIB = SIN(PHIB*DEG2RAD)
```

```
      SINTHB = SIN(THETAB*DEG2RAD)
      C1 = K*SINTHB*COSPHIB
      C2 = K*SINTHB*SINPHIB
      DB = 0.4286
      DF = 0.5*DB*K1
      PI02X0 = PI / (2.0*X0)
      PI02Y0 = PI / (2.0*Y0)
      NC = C / 2.0
      CALL SSWTCH(4, MSW)
      IF(MSW .EQ. 2)  PRINT 607,  PHI
      OO = (0.0, 0.0)
      DO 10  N=1,7
      ARGR = AMPL(N+7,IFB)*COS(ANGLE(N+7,IFB)*DEG2RAD)
      ARGI = AMPL(N+7,IFB)*SIN(ANGLE(N+7,IFB)*DEG2RAD)
      OC = OO + CMPLX(ARGR, ARGI)
      ARGR = AMPL(N,IFB)*COS(ANGLE(N,IFB)*DEG2RAD)
      ARGI = AMPL(N,IFB)*SIN(ANGLE(N,IFB)*DEG2RAD)
   10 CF(N) = CMPLX(ARGR, ARGI)
      OKV = (EPS - 1.0) * CF * OO
      THETAO = THETAL
      COSRTH = COS(RTHETA*DEG2RAD)
      SINRTH = SIN(RTHETA*DEG2RAD)
      DELTA = AMAX1( (X0 - Y0*COSRTH/SINRTH), 0.0)
      L4 = INT(X0/DEL)
      L3 = INT(DELTA/DEL)
      L2 = -L3
      L1 = -L4
      WW(1) = -Y0 / SINRTH      $WW(2) = -Y0 / SINRTH
      TT(2) =  Y0 / SINRTH      $TT(3) =  Y0 / SINRTH
      UU(2) = -Y0 / SINRTH      $UU(3) = -Y0 / SINRTH
      SS(1) =  Y0 / SINRTH      $SS(2) =  Y0 / SINRTH
C
C     BEGIN THETA LOOP
C
   20 CONTINUE
      CALL SSWTCH(6, JSW)
      IF(JSW .EQ. 1)  STOP
      THETA = THETAO + DEG2RAD
      COSTH = COS(THETA)
      SINTH = SIN(THETA)
      OKH = (0.0, 0.0)
      DO 30  N=1,7
   30 OKH = OF(N)*CEXP(CMPLX(0.0,-CF*FLOAT(2*N-1)*(1.0-COSTH) ) ) + OKH
      OKH = (EPS - 1.0) * CF * OKH
      OK  = 0.53*OKH + 0.85*OKV
      ALPHA1 = K*SINTH*COSPHI + PI02X0 - C1
      ALPHA2 = K*SINTH*COSPHI - PI02X0 - C1
      BETA1  = K*SINTH*SINPHI + PI02Y0 - C2
      BETA2  = K*SINTH*SINPHI - PI02Y0 - C2
      NN2 = 2*NN
      N2  = -NN2
      Q1  = (0.0, 0.0)      $Q2 = (0.0, 0.0)
      IF(ITYPE .EQ. 2)  GO TO 35
      S1 = ((CCS(ENN*ALPHA1*DEL) - COS( (ENN+0.5)*ALPHA1*DEL) )/(1.0 -
     1   COS(0.5*ALPHA1*DEL) )
      S2 = ((CCS(ENN*ALPHA2*DEL) - COS( (ENN+0.5)*ALPHA2*DEL) )/(1.0 -
     1   COS(0.5*ALPHA2*DEL) )
```

```
      Q1 = CMPLX(S1, 0.0)      $Q2 = CMPLX(S2, 0.0)
      GO TO 38
C
C     BEGIN N2 LOOP1
C
   35 ARG = H * SIN(0.5*FLOAT(N2)*DEL/H)
      Q1 = CEXP(CMPLX(0.0, ALPHA1*ARG) ) + Q1
      Q2 = CEXP(CMPLX(0.0, ALPHA2*ARG) ) + Q2
      N2 = N2 + 1
      IF(N2 .LE. NN2)  GO TO 35
C
C     END OF N2 LOOP
C
   38 TERM1 = SIN(BETA1*Y0)/BETA1 + SIN(BETA2*Y0)/BETA2
      QFH = (Q1*SIN(HD*ALPHA1)/ALPHA1 + Q2*SIN(HD*ALPHA2)/ALPHA2) *
     1   TERM1 * QKH
      P0  = (SIN(ALPHA1*X0)/ALPHA1 + SIN(ALPHA2*X0)/ALPHA2) * TERM1
      GAMMA1 =  ALPHA1*SINRTH - BETA1*COSRTH
      PHC1   =  ALPHA1*SINRTH + BETA1*COSRTH
      GAMMA2 =  ALPHA1*SINRTH - BETA2*COSRTH
      PHC2   =  ALPHA1*SINRTH + BETA2*COSRTH
      GAMMA3 =  ALPHA2*SINRTH - BETA1*COSRTH
      PHC3   =  ALPHA2*SINRTH + BETA1*COSRTH
      GAMMA4 =  ALPHA2*SINRTH - BETA2*COSRTH
      PHC4   =  ALPHA2*SINRTH + BETA2*COSRTH
      LAMBDA1 =  ALPHA1*COSRTH + BETA1*SINRTH
      XI1    = -ALPHA1*COSRTH + BETA1*SINRTH
      LAMBDA2 =  ALPHA1*COSRTH + BETA2*SINRTH
      XI2    = -ALPHA1*COSRTH + BETA2*SINRTH
      LAMBDA3 =  ALPHA2*COSRTH + BETA1*SINRTH
      XI3    = -ALPHA2*COSRTH + BETA1*SINRTH
      LAMBDA4 =  ALPHA2*COSRTH + BETA2*SINRTH
      XI4    = -ALPHA2*COSRTH + BETA2*SINRTH
      N = -NN
      QFM = (0.0, 0.0)
      QFF = (0.0, 0.0)
C
C     BEGIN M LOOP
C
   40 XN = FLOAT(N) * DEL
      IF(ITYPE .EQ. 2)  XN = H * SIN(XN/H)
      IF(N .GE. L3  .AND.  N .LE. L4)  GO TO 80
      IF(N .GE. L2  .AND.  N .LT. L3)  GO TO 60
      IF(N .GE. L1  .AND.  N .LT. L2)  GO TO 70
   50 J = 1
      TT(1) = (X0 - XN) / COSRTH
      UU(1) = -TT(1)
      GO TO 90
   60 J = 2
      GO TO 90
   70 J = 3
      WW(3) = -(X0 + XN) / COSRTH
      SS(3) = -WW(3)
   80 QE1 = CEXP( CMPLX(0.0, ALPHA1*XN) )
      QE2 = CEXP( CMPLX(0.0, ALPHA2*XN) )
      S = SS(J)
      T = TT(J)
```

```
      U = UU(J)
      W = WW(J)
      QPS =(CMPLX(0.0,(SIN(HD*GAMMA1)/(GAMMA1*LAMBDA1)))*QF(LAMBDA1,T,W)
     1+CMPLX(0.0,(SIN(HD*GAMMA2)/(GAMMA2*LAMBDA2)))*QF(LAMBDA2,T,W))*QE1
     2+(CMPLX(0.0,(SIN(HD*GAMMA3)/(GAMMA3*LAMBDA3)))*QF(LAMBDA3,T,W)
     3+CMPLX(0.0,(SIN(HD*GAMMA4)/(GAMMA4*LAMBDA4)))*QF(LAMBDA4,T,W))*QE2
      QPP = QPP - QPS
      QPM = -QE1*(CMPLX(0.0,(SIN(HD*RHO1)/(RHO1*XI1)))*QF(XI1,S,U) +
     1            CMPLX(0.0,(SIN(HD*RHO2)/(RHO2*XI2)))*QF(XI2,S,U))
     2      -QE2*(CMPLX(0.0,(SIN(HD*RHO3)/(RHO3*XI3)))*QF(XI3,S,U) +
     3            CMPLX(0.0,(SIN(HD*RHO4)/(RHO4*XI4)))*QF(XI4,S,U))+QPM
      N = N + 1
      IF(N .LE. NM)  GO TO 40
C
C     END OF N LOOP
C
      QPP = CMPLX(0.5, 0.0) * QK * QPP
      QPM = CMPLX(0.5, 0.0) * QK * QPM
      TERM2 = 1.0 - (SINTH*SINPHI)**2
      IF(TERM2 .LT. 1.0E-20)  TERM2 = 1.0E-20
      PV  = TERM2 * PD**2
      PV  = 10.0 * ALOG10( PV )
      PR  = TERM2*CABS( CMPLX(PD, 0.0) + CEXP( CMPLX(0.0, K*H*COSTH) )*
     1     (QPM + QPM + QPP) )**2
      PR  = 10.0 * ALOG10( PR )
      PRINT 610,  THETAD, PV, PR
      THETAD = THETAD + DELTH
      IF(THETAD .LE. THETAU)  GO TO 20
C
C     END OF THETA LOOP
C
  600 FORMAT(1H1,T15,6HPHI = ,F6.2/1H0,T5,5HTHETA,12X,2HPV,1EX,2HPR/)
  610 FORMAT(F10.3,1P2E18.7)
      END
```

MISSION
of
Rome Air Development Center

RADC plans and conducts research, exploratory and advanced development programs in command, control, and communications (C^3) activities, and in the C^3 areas of information sciences and intelligence. The principal technical mission areas are communications, electromagnetic guidance and control, surveillance of ground and aerospace objects, intelligence data collection and handling, information system technology, ionospheric propagation, solid state sciences, microwave physics and electronic reliability, maintainability and compatibility.

Printed by
United States Air Force
Hanscom AFB, Mass. 01731